CHALMERS | UNIVERSITY OF GOTHENBURG

PREPRINT 2008:36

An adaptive finite element method for second order plate theory

PETER HANSBO
DAVID HEINTZ
MATS G. LARSON

Department of Mathematical Sciences
Division of Mathematics
CHALMERS UNIVERSITY OF TECHNOLOGY
UNIVERSITY OF GOTHENBURG
Göteborg Sweden 2008

Preprint 2008:36

An adaptive finite element method for second order plate theory

Peter Hansbo, David Heintz and Mats G. Larson

Department of Mathematical Sciences
Division of Mathematics
Chalmers University of Technology and University of Gothenburg
SE-412 96 Göteborg, Sweden
Göteborg, November 2008

Preprint 2008:36
ISSN 1652-9715

Matematiska vetenskaper
Göteborg 2008

An adaptive finite element method for second order plate theory

Peter Hansbo[1], David Heintz[1] and Mats G. Larson[2]

[1] *Department of Mathematics, Chalmers University of Technology and University of Gothenburg, SE–412 96 Göteborg, Sweden*

[2] *Department of Mathematics and Mathematical Statistics, Umeå University, SE–901 87 Umeå, Sweden*

Abstract

We present a discontinuous finite element method for the Kirchhoff plate model with membrane stresses. The method is based on P^2-approximations on simplices for the out-of-plane deformations, using C^0-continuous approximations. We derive *a posteriori* error estimates for linear functionals of the error and give some numerical examples.

1 INTRODUCTION

Kirchhoff plate deformation analysis is often carried out without taking into account the effect of in-plane stresses. However, if these are significant or if a stability analysis is required, the fourth order plate equations must be supplemented with a second order term. In such a case, standard finite element methods for plates may not be well suited for the problem; an example of this is the well known Morley plate element which is known not to converge for the Laplace equation, cf. [7]. In this paper we instead use the continuous/discontinuous Galerkin method first proposed by Engel et al. [2], and proposed (using a different but related formulation) for second order theory by Wells and Dung [8]. In this paper, we focus on using continuous piecewise second degree polynomials (with discontinuous derivatives) for the plate and constant–strain elements for the in-plane deformations. We present an *a posteriori* error analysis including the modeling error in the stresses. The total error is thus composed of two parts: the plate discretization error and the error emanating from the modeling of the stresses. In our case the stress

error is also a discretization error, which allows for *a posteriori* control of the total error. However, the separation of the errors allows for the use, e.g., of measured stresses, in which case some other control of the error in stresses must be used if a reliable estimate is to be obtained.

2 THE PLATE MODEL

Consider a domain $\Omega \subset \mathbb{R}^2$, for simplicity assumed to be a convex polygon, whose boundary $\partial\Omega$ has an outward pointing normal $\boldsymbol{n}$. The plate thickness in the out-of-plane x_3-direction is denoted by t, and the deflection in the x_3-direction by u. The differential equations describing the Kirchhoff plate model with membrane stresses can be derived from minimization of the sum of the bending energy and the potential of the surface and in-plane stress load,

$$\mathcal{U}_z(u) = \frac{D}{2}\int_\Omega \left(\left(\frac{\partial^2 u}{\partial x_1^2} + \frac{\partial^2 u}{\partial x_2^2} \right)^2 - 2\,(1-\nu) \left(\frac{\partial^2 u}{\partial x_1^2}\frac{\partial^2 u}{\partial x_2^2} - \left(\frac{\partial^2 u}{\partial x_1 \partial x_2} \right)^2 \right) \right) d\Omega + \frac{t}{2}\int_\Omega \left(\sigma_{11} \left(\frac{\partial u}{\partial x_1} \right)^2 + \sigma_{22} \left(\frac{\partial u}{\partial x_2} \right)^2 + 2\sigma_{12} \frac{\partial u}{\partial x_1}\frac{\partial u}{\partial x_2} \right) d\Omega - \int_\Omega g\, u\, d\Omega \tag{1}$$

where g is the transverse surface load,

$$\boldsymbol{\sigma} = \begin{bmatrix} \sigma_{11} & \sigma_{12} \\ \sigma_{12} & \sigma_{22} \end{bmatrix}$$

is the in-plane stress tensor, given by the solution to the plane stress problem

$$\begin{aligned} -\nabla \cdot \boldsymbol{\sigma} &= \boldsymbol{f} \quad \text{in } \Omega, \\ \boldsymbol{\sigma} &= \boldsymbol{\sigma}(\boldsymbol{u}) := 2\mu\boldsymbol{\varepsilon}(\boldsymbol{u}) + \lambda\, \nabla \cdot \boldsymbol{u}\, \boldsymbol{1}, \end{aligned}$$

where $\lambda = E\nu/(1-\nu^2)$ and $\mu = E/(2\,(1+\nu))$; $D = Et^3/(12(1-\nu^2))$ is the flexural rigidity of the plate, and E and ν are Young's modulus and Poisson's ratio, respectively.

In the following, we shall assume that if the stresses are compressive, they are small enough to ensure coercivity of the full problem; the case of large compressive stresses occurs in the analysis of plate buckling, where the potential energy functional switches from being convex to being concave, resulting in instability.

By introducing the curvature tensor

$$\boldsymbol{\kappa}(u) := \begin{bmatrix} \dfrac{\partial^2 u}{\partial x_1^2} & \dfrac{\partial^2 u}{\partial x_1 \partial x_2} \\ \dfrac{\partial^2 u}{\partial x_1 \partial x_2} & \dfrac{\partial^2 u}{\partial x_2^2} \end{bmatrix}$$

the Lamé–type parameters $\mu_{\rm P} := D(1-\nu)/2$, and $\lambda_{\rm P} := D\nu$, and the moment tensor

$$\boldsymbol{M}(u) := 2\mu_{\rm P}\boldsymbol{\kappa}(u) + \lambda_{\rm P}\Delta u\,\mathbf{1}$$

where $\mathbf{1}$ is the identity tensor, we may rewrite (1) as

$$\mathcal{U}(u) = \frac{1}{2}\int_\Omega \left(\boldsymbol{M}(u) : \boldsymbol{\kappa}(u) + t\,(\boldsymbol{\sigma}\nabla u)\cdot\nabla u - 2gu\right)\,d\Omega \tag{2}$$

where $\boldsymbol{M} : \boldsymbol{\kappa} = \sum_{ij} M_{ij}\kappa_{ij}$ denotes the contraction of two tensors. Minimization of (2) yields the plate equation with second order effects

$$\sum_{ij}\left(\frac{\partial^2 M_{ij}(u)}{\partial x_i \partial x_j} - \frac{\partial}{\partial x_i}\left(t\sigma_{ij}\frac{\partial u}{\partial x_j}\right)\right) = g \quad \text{in } \Omega, \tag{3}$$

supplied with the appropriate boundary conditions.

For simplicity, we shall restrict the presentation to the case of clamped boundary conditions: $\boldsymbol{n}\cdot\nabla u = 0$ and $u = 0$ on $\partial\Omega$. We shall also assume that the constitutive parameters and the thickness are constant.

3 THE FINITE ELEMENT METHOD

3.1 Variational formulation

The virtual work equation related to (3) is the following variational statement: find

$$u \in V := \{v :\ v \in H^2(\Omega), v = 0 \text{ on } \partial\Omega,\ \boldsymbol{n}\cdot\nabla v = 0 \text{ on } \partial\Omega\}$$

such that

$$a_{\rm P}(u,v) + b(\boldsymbol{\sigma};u,v) = (g,v)$$

for all $v \in V$, where

$$a_{\rm P}(u,v) := \int_\Omega \boldsymbol{M}(u) : \boldsymbol{\kappa}(v)\,d\Omega,$$
$$b(\boldsymbol{\sigma};u,v) := t\int_\Omega (\boldsymbol{\sigma}\nabla u)\cdot\nabla v\,d\Omega.$$

To obtain $\boldsymbol{\sigma}$, we also have to solve the plane stress problem of finding $\boldsymbol{u} \in \boldsymbol{W} := [H_0^1(\Omega)]^2$ such that

$$(\boldsymbol{\sigma}(\boldsymbol{u}),\boldsymbol{\varepsilon}(\boldsymbol{v})) = (\boldsymbol{f},\boldsymbol{v}) \quad \forall \boldsymbol{v} \in \boldsymbol{W}, \tag{4}$$

where

$$(\boldsymbol{\sigma}(\boldsymbol{u}),\boldsymbol{\varepsilon}(\boldsymbol{v})) := \int_\Omega \boldsymbol{\sigma}(\boldsymbol{u}) : \boldsymbol{\varepsilon}(\boldsymbol{v})\,d\Omega$$

In the following, we shall also use the L_2 scalar product notation

$$(u,v)_E := \int_E u\,v\,ds, \quad (\boldsymbol{M},\boldsymbol{\tau})_T := \int_T \boldsymbol{M} : \boldsymbol{\tau}\,dxdy, \quad \text{etc.}$$

If the subscript is omitted, the product is taken over Ω.

3.2 Finite element method

We consider a subdivision $\mathcal{T} = \{T\}$ of Ω into a geometrically conforming, quasiuniform, simplicial finite element mesh. Denote by h_T the diameter of element T and by $h = \max_{T\in\mathcal{T}} h_T$ the global mesh size parameter. We shall use continuous, piecewise polynomial, approximations of the transverse displacement:

$$V_h := \{v \in H_0^1(\Omega) \cap C^0(\Omega) : \ v|_T \in P^2(T),\ \forall T \in \mathcal{T}\}.$$

To define our methods we introduce the set of edges in the mesh, $\mathcal{E} = \{E\}$, and we split $\mathcal{E}$ into two disjoint subsets

$$\mathcal{E} = \mathcal{E}_I \cup \mathcal{E}_B,$$

where $\mathcal{E}_I$ is the set of edges in the interior of Ω and $\mathcal{E}_B$ is the set of edges on the boundary. Further, with each edge we associate a fixed unit normal $\boldsymbol{n}$ such that for edges on the boundary $\boldsymbol{n}$ is the exterior unit normal. We denote the jump of a function $\boldsymbol{v} \in \boldsymbol{\Gamma}_h$ at an edge E by $[\boldsymbol{v}] = \boldsymbol{v}^+ - \boldsymbol{v}^-$ for $E \in \mathcal{E}_I$ and $[\boldsymbol{v}] = \boldsymbol{v}^+$ for $E \in \mathcal{E}_B$, and the average $\langle \boldsymbol{v} \rangle = (\boldsymbol{v}^+ + \boldsymbol{v}^-)/2$ for $E \in \mathcal{E}_I$ and $\langle \boldsymbol{v} \rangle = \boldsymbol{v}^+$ for $E \in \mathcal{E}_B$, where $\boldsymbol{v}^\pm = \lim_{\epsilon\downarrow 0} \boldsymbol{v}(\boldsymbol{x} \mp \epsilon\, \boldsymbol{n})$ with $\boldsymbol{x} \in E$.

Our method can now be formulated as follows: find $u_h \in V_h$ such that

$$a_{\mathrm{P}}^h(u_h, v) + b(\boldsymbol{\sigma}; u_h, v) = (g, v) \tag{5}$$

for all $v \in V_h$. In (5) the bilinear form $a_{\mathrm{P}}^h(\cdot,\cdot)$ is defined on V_h as follows

$$\begin{aligned} a_{\mathrm{P}}^h(u, v) = &\sum_{T\in\mathcal{T}} (\boldsymbol{M}(u), \boldsymbol{\kappa}(v))_T \\ &- \sum_{E\in\mathcal{E}_I\cup\mathcal{E}_B} (\langle \boldsymbol{n}\cdot\boldsymbol{M}(u)\cdot\boldsymbol{n}\rangle, [\boldsymbol{n}\cdot\nabla v])_E \\ &- \sum_{E\in\mathcal{E}_I\cup\mathcal{E}_B} (\langle \boldsymbol{n}\cdot\boldsymbol{M}(v)\cdot\boldsymbol{n}\rangle, [\boldsymbol{n}\cdot\nabla u])_E \\ &+ (2\mu + 2\lambda)\,\gamma_0 \sum_{E\in\mathcal{E}_I\cup\mathcal{E}_B} h_E^{-1} ([\boldsymbol{n}\cdot\nabla u], [\boldsymbol{n}\cdot\nabla v])_E \end{aligned}$$

Here γ_0 is a constant whose role is to enforce coercivity of the form $a_{\mathrm{P}}^h(\cdot,\cdot)$, and h_E is defined by

$$h_E = \left(|T^+| + |T^-|\right)/(2\,|E|) \quad \text{for } E = \partial T^+ \cap \partial T^-, \tag{6}$$

with $|T|$ the area of T, on each edge. Precise values for the choice of γ_0 are given in [5].

Using Green's formula, we readily establish the following Lemma.

Lemma 1 *The method* (5) *is consistent in the sense that*

$$a_{\mathrm{P}}^h(u-u_h,v)+b(\boldsymbol{\sigma};u-u_h,v)=0 \tag{7}$$

for all $v\in V_h$.

Now, the $\boldsymbol{\sigma}$ in (5) is the exact stress solution to the problem (4) which we cannot solve exactly in general. Instead we introduce the discrete problem of finding $\boldsymbol{u}_h\in\boldsymbol{W}_h$, where

$$\boldsymbol{W}_h:=\{\boldsymbol{v}\in\boldsymbol{W}\cap[C^0(\Omega)]^2:\ \boldsymbol{v}|_T\in[P^1(T)]^2,\ \forall T\in\mathcal{T}\},$$

such that

$$(\boldsymbol{\sigma}(\boldsymbol{u}_h),\boldsymbol{\varepsilon}(\boldsymbol{v}))=(\boldsymbol{f},\boldsymbol{v})\quad\forall\boldsymbol{v}\in\boldsymbol{W}_h. \tag{8}$$

Using the notation $\boldsymbol{\sigma}_h:=\boldsymbol{\sigma}(\boldsymbol{u}_h)$, our discrete plate problem becomes: find $u_h\in V_h$ such that

$$a_{\mathrm{P}}^h(u_h,v)+b(\boldsymbol{\sigma}_h;u_h,v)=(g,v) \tag{9}$$

for all $v\in V_h$, and the orthogonality relation (7) is weakened to

$$a_{\mathrm{P}}^h(u-u_h,v)+b(\boldsymbol{\sigma};u,v)-b(\boldsymbol{\sigma}_h;u_h,v)=0,\quad\forall v\in V_h. \tag{10}$$

3.3 An approach to *a posteriori* error estimation

Since the error in the discrete plate problem (9) does not couple to the plane stress problem (8), we shall here follow Larson and Bengzon [3] and view the fact that we must replace $\boldsymbol{\sigma}$ by $\boldsymbol{\sigma}_h$ as a *modeling error*.

Following Becker and Rannacher [1], we are interested in controlling a linear functional $L(u-u_h)$ of the error (where L is to be specified), and to this end we introduce the dual problem of finding z such that

$$\sum_{ij}\left(\frac{\partial^2 M_{ij}(z)}{\partial x_i\partial x_j}-\frac{\partial}{\partial x_i}\left(t\sigma_{ij}^h\frac{\partial z}{\partial x_j}\right)\right)=J\quad\text{in }\Omega, \tag{11}$$

$z=0$ and $\boldsymbol{n}\cdot\nabla z=0$ on $\partial\Omega$. Here J is the Riesz representer of L, $L(v)=(J,v)$. Then, since $[\boldsymbol{n}\cdot\nabla z]=0$ on the edges,

$$\begin{aligned}(J,e)=L(u-u_h)&=a_{\mathrm{P}}^h(z,u-u_h)+b(\boldsymbol{\sigma}_h;z,u-u_h)\\&=a_{\mathrm{P}}^h(u-u_h,z)+b(\boldsymbol{\sigma}_h;u-u_h,z)+b(\boldsymbol{\sigma};u,z)-b(\boldsymbol{\sigma};u,z)\\&=(g,z-\pi_h z)-a_{\mathrm{P}}^h(u_h,z-\pi_h z)-b(\boldsymbol{\sigma}_h;u_h,z-\pi_h z)\\&\quad+b(\boldsymbol{\sigma}_h-\boldsymbol{\sigma};u,z),\end{aligned} \tag{12}$$

where we used (10) in the last step.

Since $\boldsymbol{\sigma} - \boldsymbol{\sigma}_h = \boldsymbol{\sigma}(\boldsymbol{u} - \boldsymbol{u}_h)$, we can now introduce a second functional, related to the modelling error.

$$L_{\text{mod}}(\boldsymbol{u} - \boldsymbol{u}_h) := -b(\boldsymbol{\sigma}(\boldsymbol{u} - \boldsymbol{u}_h); u, z)$$

and the dual problem of finding $\boldsymbol{z} \in \boldsymbol{W}$ such that

$$(\boldsymbol{\sigma}(\boldsymbol{v}), \boldsymbol{\varepsilon}(\boldsymbol{z})) = L_{\text{mod}}(\boldsymbol{v}) \quad \forall \boldsymbol{v} \in \boldsymbol{W}.$$

Thus, the functional L_{mod} of the error can be evaluated as

$$\begin{aligned} L_{\text{mod}}(\boldsymbol{u} - \boldsymbol{u}_h) &= (\boldsymbol{\sigma}(\boldsymbol{u} - \boldsymbol{u}_h), \boldsymbol{\varepsilon}(\boldsymbol{z})) \\ &= (\boldsymbol{f}, \boldsymbol{z} - \pi_h \boldsymbol{z}) - (\boldsymbol{\sigma}_h, \boldsymbol{\varepsilon}(\boldsymbol{z} - \pi_h \boldsymbol{z})), \end{aligned}$$

where we used that

$$(\boldsymbol{\sigma}(\boldsymbol{u}) - \boldsymbol{\sigma}(\boldsymbol{u}_h), \boldsymbol{\varepsilon}(\boldsymbol{v})) = 0, \quad \forall \boldsymbol{v} \in \boldsymbol{W}_h.$$

In conclusion, we have that

$$\begin{aligned} L(u - u_h) = (g, z - \pi_h z) - a_{\text{P}}^h(u_h, z - \pi_h z) - b(\boldsymbol{\sigma}_h; u_h, z - \pi_h z) \\ + (\boldsymbol{f}, \boldsymbol{z} - \pi_h \boldsymbol{z}) - (\boldsymbol{\sigma}_h, \boldsymbol{\varepsilon}(\boldsymbol{z} - \pi_h \boldsymbol{z})). \end{aligned} \tag{13}$$

In (13), the error contribution has thus been split between discretization errors for the plate (the terms involving $z - \pi_h z$) and the model error (in this case discretization error) in the stresses (the terms involving $\boldsymbol{z} - \pi_h \boldsymbol{z}$). The continuous stresses do not enter directly into the discretization error for the plate; the effect of using approximate stresses has been separated out. In case the stresses have been obtained in some other way, e.g., by measurement, (12) can instead be used together with some direct estimate of the stress error.

4 IMPLEMENTATION

We seek to establish a practical adaptive scheme, such that a linear functional $L(\cdot)$ of the error, $e = u - u_h$, is bounded. To that end, duality-based techniques are employed, which include solving enriched problems—the corresponding dual problems—to distribute degrees of freedom in an efficient manner. In our numerical examples, the datum of the dual plate problem (11), i.e., the target quantity, is chosen as a Dirac delta function

$$J := \delta(x_1 - \bar{x}_1, x_2 - \bar{x}_2), \tag{14}$$

where $(\bar{x}_1, \bar{x}_2)$ is the node of maximum plate deflection (whose location is expected to converge rather quickly as the mesh size $h \to 0$). As opposed to estimating the error with respect to global energy norms or global L_2-norms,

(14) exemplifies a typical local quantity, which often is more appropriate in applications.

The linear functional (13) was written as a sum, $L(e) = \eta_{\mathrm{P}} + \eta_{\mathrm{M}}$, where

$$\eta_{\mathrm{P}} = (g, z - \pi_h z) - a_{\mathrm{P}}^h(u_h, z - \pi_h z) - b(\boldsymbol{\sigma}_h; u_h, z - \pi_h z), \tag{15}$$

$$\eta_{\mathrm{M}} = (\boldsymbol{f}, \boldsymbol{z} - \pi_h \boldsymbol{z}) - (\boldsymbol{\sigma}_h, \boldsymbol{\varepsilon}(\boldsymbol{z} - \pi_h \boldsymbol{z})), \tag{16}$$

represent the effects of the discretization and model errors. This provides alternatives for the discretization of the domain Ω:

(i) use a common partition $\mathcal{T}$ (quadratic and linear triangles for the plate and plane stress problems coincide geometrically);

(ii) use disparate triangulations $\mathcal{T}_{\mathrm{P}}$ and $\mathcal{T}_{\mathrm{M}}$.

The first option associates each element $T_i \in \mathcal{T}$ with an error indicator

$$\eta^i = |\eta_{\mathrm{P}}^i| + |\eta_{\mathrm{M}}^i|, \quad i = 1, 2, \ldots, N, \tag{17}$$

where N is the number of elements of $\mathcal{T}$. This choice makes for an easier implementation, but the information from (15) and (16) is not thoroughly exploited, since we resort to sums of local errors contributions. The more flexible approach—in keeping with model adaptivity—would be a direct comparison, made possible by disparate triangulations. However, this necessitates making searches when solving the *point-in-triangle* problem (see, e.g., [9, Algorithm 4]), usually preceded by constructing a suitable search structure, a so-called *binary tree* or *quad tree*; we refer to [10] for further details. In the present context, the need for such searches typically arise when basis functions are evaluated in abscissas (query points), situated on different elements (targets) between $\mathcal{T}_{\mathrm{P}}$ and $\mathcal{T}_{\mathrm{M}}$.

Remark 1 *Preprocessing Ω into a search structure comes at a cost, and although intended to ease the effort, it still takes time to perform searches (the procedure ought to be parallelized since individual queries are independent). The winnings are increased flexibility in distributing the degrees of freedom, thereby yielding smaller matrix problems achieving the same level of accuracy.*

In the sequel the discussion focuses on using disparate meshes (the other case being a reduced analog), where $\mathcal{T}_{\mathrm{P}}$ and $\mathcal{T}_{\mathrm{M}}$ are assumed to consist of N_{P} and N_{M} elements, respectively. Hence, instead of (17), consider the concatenated $(N_{\mathrm{P}} + N_{\mathrm{M}})$-tuple

$$\eta = \big(\eta_{\mathrm{P}}^1, \ldots, \eta_{\mathrm{P}}^{N_{\mathrm{P}}}, \eta_{\mathrm{M}}^1, \ldots, \eta_{\mathrm{M}}^{N_{\mathrm{M}}}\big), \tag{18}$$

from which we select a fixed ratio r of the largest absolute local error indicators, regardless of the error source, and mark the corresponding elements for

refinement. The primal meshes are updated via a Bänsch-algorithm (longest edge bisection) leaving no hanging nodes.

In order to determine (18) we need to approximate exact solutions. Therefore we introduce two auxiliary problems: Find $\tilde{u} \in V_h^*$ and $\tilde{z} \in V_h^*$ such that

$$\begin{aligned} a_{\mathrm{P}}^h(\tilde{u}, v) + b(\boldsymbol{\sigma}_h; \tilde{u}, v) &= (g, v), \quad \forall v \in V_h^*, \\ a_{\mathrm{P}}^h(v, \tilde{z}) + b(\boldsymbol{\sigma}_h; v, \tilde{z}) &= L(v), \quad \forall v \in V_h^*, \end{aligned}$$

which assemble the same stiffness matrix, only deviating by the RHS-data (thus passed together as arguments to a direct sparse Cholesky solver). The solutions are then used as input to the discretized dual plane stress problem: Find $\tilde{\boldsymbol{z}} \in \boldsymbol{W}_h^*$ such that

$$(\boldsymbol{\sigma}(\boldsymbol{v}), \boldsymbol{\varepsilon}(\tilde{\boldsymbol{z}})) = -b(\boldsymbol{\sigma}(\boldsymbol{v}); \tilde{u}, \tilde{z}), \quad \forall \boldsymbol{v} \in \boldsymbol{W}_h^*.$$

The enriched function spaces $V_h^* \supset V_h$ and $\boldsymbol{W}_h^* \supset \boldsymbol{W}_h$ are constructed by subjecting the primal partitions to regular subdivision, leading to the refined triangulations $\tilde{\mathcal{T}}_{\mathrm{P}}$ and $\tilde{\mathcal{T}}_{\mathrm{M}}$, respectively. When calculating local error indicators by (15) and (16), $\pi_h v : V_h^* \to V_h$ and $\pi_h \boldsymbol{v} : \boldsymbol{W}_h^* \to \boldsymbol{W}_h$ were taken, for simplicity, to be nodal interpolation operators.

The stopping criterion of the adaptive algorithm is imposed on the relative error

$$e_{\mathrm{rel}} := \left| \frac{L(\tilde{e})}{\tilde{u}(\bar{x}_1, \bar{x}_2)} \right| \leq \mathrm{TOL},$$

where

$$L(\tilde{e}) = L_{\mathrm{P}} + L_{\mathrm{M}}, \quad L_{\mathrm{P}} = \sum_{j=1}^{N_{\mathrm{P}}} \eta_{\mathrm{P}}^j, \; L_{\mathrm{M}} = \sum_{k=1}^{N_{\mathrm{M}}} \eta_{\mathrm{M}}^k,$$

and TOL is a prescribed tolerance. Furthermore, let

$$|L_{\mathrm{P}}| = \sum_{j=1}^{N_{\mathrm{P}}} |\eta_{\mathrm{P}}^j|, \quad |L_{\mathrm{M}}| = \sum_{k=1}^{N_{\mathrm{M}}} |\eta_{\mathrm{M}}^k|,$$

denote the sums of the absolute local error indicators. The adaptive scheme is summarized in Algorithm 1.

Remark 2 *The bilinear form a_P^h contains a penalty term, controlling the normal derivative, which is scaled by a parameter γ_0. From [5] a lower bound of $\gamma_0 > 3C_I$, where C_I is a constant that depends on the order k of the approximation, ensures its coercivity. For this purpose we set $\gamma_0 = 3/2$ in all test problems, using the asymptotic value of the constant.*

The a posteriori error estimator is evaluated in terms of the effectivity index

$$\theta := \left| \frac{L(\tilde{e})}{L(\hat{e})} \right| = \left| \frac{L(\tilde{e})}{\hat{u}(\bar{x}_1, \bar{x}_2) - u_h(\bar{x}_1, \bar{x}_2)} \right|,$$

Algorithm 1: Adaptive scheme

Data: initial mesh $\mathcal{T}^0$, user-specified tolerance TOL
Result: FE-solution u_h, total error $L(\tilde{e})$

for $i = 0, 1, \ldots$ **do**
  solve primal plane stress problem for $\boldsymbol{\sigma}_h$ on $\mathcal{T}_{\mathrm{M}}^i$
  solve primal plate problem for u_h on $\mathcal{T}_{\mathrm{P}}^i$
  construct dual meshes $\tilde{\mathcal{T}}_{\mathrm{P}}^i$ and $\tilde{\mathcal{T}}_{\mathrm{M}}^i$
  solve primal and dual plate problems for $\tilde{u}$ and $\tilde{z}$ on $\tilde{\mathcal{T}}_{\mathrm{P}}^i$
  solve dual plane stress problem for $\tilde{\boldsymbol{z}}$ on $\tilde{\mathcal{T}}_{\mathrm{M}}^i$
  compute local error indicators η_{P}^j and η_{M}^k
  if TOL $> e_{\mathrm{rel}}$ **then**
    refine primal meshes: $\mathcal{T}_{\mathrm{P}}^i \to \mathcal{T}_{\mathrm{P}}^{i+1}$, $\mathcal{T}_{\mathrm{M}}^i \to \mathcal{T}_{\mathrm{M}}^{i+1}$
  else
    break
  end
end

where $\hat{u}(\bar{x}_1, \bar{x}_2)$ is a reference solution replacing the unknown exact maximum plate deflection. $\hat{u}$ was obtained by solving the primal problems adaptively on a common dense mesh $\hat{\mathcal{T}}$.

The adaptive procedure is rather time-consuming—in every iteration two dual problems are solved (including the enhanced discrete plate problem). An effort to reduce the computational cost would be to solve the problems with respect to their primal FE-spaces, followed by post-processing to obtain solutions in enriched function spaces, see, e.g., Larsson et al. [6].

5 NUMERICAL EXAMPLES

Algorithm 1 is applied to a set of test problems, which is not meant to be comprehensive, but to exemplify the behavior of the a posteriori error estimator. We shall compare two adaptive strategies: 1) refine a common mesh $\mathcal{T}^i$ (referred to as the CM-method); and 2) refine disparate meshes $\mathcal{T}_{\mathrm{P}}^i$ and $\mathcal{T}_{\mathrm{M}}^i$ (DM-method). Note that

- the transversal and in-plane boundary conditions are different in each setup;
- the load—either $\boldsymbol{f}$ or $\boldsymbol{g}$—causing the stress field $\boldsymbol{\sigma}$ is restricted to maintain the positive-definiteness of the stiffness matrix (typically the loading must not be too large);
- the refinement ratio is set to $r = 0.2$.

Remark 3 *The computational cost—per degree of freedom—associated with the plate problem is larger (than for the plane stress problem), partly due to the symmetry and penalty terms of the a_P^h-functional, alongside the additional b-functional. Consequently, having a relatively small plate problem could be beneficial, and hence relevant results are presented with respect to: 1) the total number of degrees of freedom $D_T = D_P + D_M$; and 2) the number of degrees of freedom for the plate problem D_P.*

5.1 Point Load on Unit Square

Consider the plate $\Omega = [0,1] \times [0,1]$, simply supported (so that $u = 0$ at $\partial\Omega$) and fixed on the left side ($\boldsymbol{u}|_{x_1=0} = \mathbf{0}$). The material parameters are $\nu = 0.3$, $E = 100$, and the thickness $t = 0.1$. The plate carries a point load at $\boldsymbol{x}_l = (1/4,\, 3/4)$, whereas in-plane stresses are induced by a surface traction $\boldsymbol{g} = (0,\, -1)$ at $x_2 = 1$.

The plane stress FE-formulation now becomes: Find $\boldsymbol{u}_h \in \boldsymbol{W}_h$ such that

$$(\boldsymbol{\sigma}(\boldsymbol{u}_h), \boldsymbol{v}) = (\boldsymbol{g}, \boldsymbol{v})_{\partial\Omega_\mathrm{N}}, \quad \forall \boldsymbol{v} \in \boldsymbol{W}_h,$$

where $\partial\Omega_\mathrm{N}$ denotes the Neumann boundary $x_2 = 1$, and the local model error indicator (16) changes accordingly

$$\eta_\mathrm{M} = (\boldsymbol{g}, \boldsymbol{z} - \pi_h \boldsymbol{z})_{\partial\Omega_\mathrm{N}} - (\boldsymbol{\sigma}_h, \boldsymbol{\varepsilon}(\boldsymbol{z} - \pi_h \boldsymbol{z})).$$

The point load is applied to a single node, and thus the discrete load vector $\mathbf{f}_\mathrm{P} = \delta_{ij}$, so that (15) reduces to

$$\eta_\mathrm{P} = -a_\mathrm{P}^h(u_h, z - \pi_h z) - b(\boldsymbol{\sigma}_h; u_h, z - \pi_h z).$$

The FE-solutions of the plate and plane stress problems are shown in Figures 1 and 2 (the latter uses non-deformed coordinates): the maximum plate deflection (cross-marked) is situated close to $\boldsymbol{x}_l$ (circle-marked), whereas large effective stresses

$$\sigma_\mathrm{e} := (\boldsymbol{\sigma} : \boldsymbol{\sigma})^{1/2}$$

appear in the vicinity of the vertices $(0,0)$, $(0,1)$.

Consecutive updates of $\mathcal{T}$ were presumably dominated by the discretization error, as implied by Table 1, where the larger and strictly decreasing L_P (almost) sums up to the total error $L(\hat{e})$ (disregarding cancellation effects). Refinements are concentrated around $\boldsymbol{x}_l$, as seen in Figure 6, and hence one anticipates $N_\mathrm{P} > N_\mathrm{M}$, should disparate meshes be used. This is also the case, being confirmed by Table 2 and Figure 14(a), showing the shift towards $\mathcal{T}_\mathrm{P}$-refinement as most prominent during the initial iterations. When comparing the two meshes in Figures 7 and 8, note the difference at the large-stress vertices, where consequently $\mathcal{T}_\mathrm{M}$ is refined while $\mathcal{T}_\mathrm{P}$ is not,

following the almost symmetric (along the line $x_2 = 1 - x_1$) refinement pattern of $\mathcal{T}$ instead (further underlining the importance of the discretization error).

The adaptive algorithm is superior to uniform refinement, according to Figures 15(a) and 15(b), where the latter indicates how the DM-method avoids unnecessary model complexity, i.e., results in a coarser mesh $\mathcal{T}_\mathrm{M}$, and still satisfies the prescribed relative error $\mathrm{TOL} = 5 \cdot 10^{-3}$.

The effectivity indices are stable—we obtain convergence rates of the same order as the underlying FE-method—and the accuracy is high ($\theta \to 1^+$ in Figure 13(a)).

5.2 An L-shaped Membrane

Let Ω be the polygon with vertices $(0,0), (c,0), (c,c), (1,c), (1,1)$ and $(0,1)$ for $c = 1/2$, having material parameters $\nu = 0.3$, $E = 100$, and the thickness $t = 0.1$. The plate is subjected to a uniform load $g = 1$, and carries an in-plane point load at the tip $\boldsymbol{x}_l = (1,1)$, such that $\boldsymbol{f}(\boldsymbol{x}_l) = (0,-4)$. It is simply supported ($u = 0$ at $\partial\Omega$) and fixed on the left side ($\boldsymbol{u}|_{x_1=0} = \mathbf{0}$).

In this setting, with the point load applied in a single node, the discretized load vector $\mathbf{f}_\mathrm{M} = \delta_{ij}$, and (16) reduces to

$$\eta_\mathrm{M} = -(\boldsymbol{\sigma}_h, \boldsymbol{\varepsilon}(\boldsymbol{z} - \pi_h \boldsymbol{z})),$$

otherwise (15) and the FE-formulations remain unchanged.

The maximum plate deflection (cross-marked in Figure 6) would occur along the symmetry line $x_2 = 1 - x_1$ (dashed), had it not been for large planar stresses at $\boldsymbol{x}_l$, and particularly around the non-convex corner singularity; thereby $\max u_h$ deviates to $(\bar{x}_1, \bar{x}_2) \approx (0.26, 0.51)$.

The influence of the large stresses implies how the model error now becomes more prominent. Tables 3 and 4 concurs that L_P and L_M are of the same order of magnitude (note that the cancellation effects are greater for the model error)—the DM-method recognizes this and concentrates refinements on $\mathcal{T}_\mathrm{M}$ (emphasized by Figure 14(b)). During the adaptive procedure additional elements are foremostly introduced at the interior corner $(1/2, 1/2)$, but $\mathcal{T}_\mathrm{P}$ is also resolved around $(\bar{x}_1, \bar{x}_2)$.

Using an adaptive algorithm is favorable, judging by Figure 16, and the solution improves as the complexity of the model increases. The tolerance was $\mathrm{TOL} = 2 \cdot 10^{-2}$.

The total error is slightly underestimated, but the effectivity indices remain fairly stable, and grow slowly (Figure 13(b) shows that $\theta \to 1^-$).

6 CONCLUDING REMARKS

We have presented a C^0 finite element element method for second-order analysis of thin plates. *A posteriori* error estimates for linear functionals of the error have been derived. Our numerical examples, focusing on controlling the error in maximum deflection, show that the estimates give effectivity indices close to unity.

References

[1] Becker R, Rannacher R. A feed-back approach to error control in finite element methods: basic analysis and examples. *East-West Journal of Numerical Mathematics* 1996; **4**:237–264.

[2] Engel G, Garikipati K, Hughes TJR, Larson MG, Mazzei L, Taylor RL. Continuous/discontinuous finite element approximations of fourth-order elliptic problems in structural and continuum mechanics with applications to thin beams and plates, and strain gradient elasticity. *Computer Methods in Applied Mechanics and Engineering* 2002; **191**:3669–3750.

[3] Larson MG, Bengzon F. Adaptive finite element approximation of multiphysics problems. *Communications in Numerical Methods in Engineering* 2008; **24**:505–521.

[4] Hansbo P, M.G. Larson MG. A discontinuous Galerkin method for the plate problem. *Calcolo* 2002; **39**:41–59.

[5] Hansbo P, Larson MG. A posteriori error estimates for continuous/discontinuous Galerkin approximations of the Kirchhoff-Love plate. Preprint (2008).

[6] Larsson F, Hansbo P, Runesson K. Strategies for computing goal-oriented *a posteriori error* measures in non-linear elasticity. *International Journal for Numerical Methods in Engineering* 2002; **55**:879–894.

[7] Nilssen TK, Tai XC, Winther R. A robust nonconforming H^2-element. *Mathematics of Computation* 2001; **70**:489–505.

[8] Wells GN, Dung, NT. A C^0 discontinuous Galerkin formulation for Kirchhoff plates. *Computer Methods in Applied Mechanics and Engineering* 2007; **196**:3370–3380.

[9] Svensson ED. Optimal search in finite element triangulations using binary trees. Preprint (Department of Mathematical Sciences, Division of Mathematics, Chalmers University of Technology and Göteborg University), 2006:21, 1652-9715.

[10] O'Rourke J. Computational geometry in C. 2:nd ed., Cambridge University Press, 1998.

TABLE 1: *Common mesh* $\mathcal{T}$

#	D_{P}	D_{M}	L_{P}	L_{M}	$L(\hat{e})$	θ
1	545	290	$2.81 \cdot 10^{-2}$	$1.26 \cdot 10^{-4}$	$3.15 \cdot 10^{-2}$	0.90
2	668	356	$2.57 \cdot 10^{-2}$	$9.90 \cdot 10^{-5}$	$2.16 \cdot 10^{-2}$	1.20
3	839	442	$1.22 \cdot 10^{-2}$	$6.33 \cdot 10^{-5}$	$1.32 \cdot 10^{-2}$	0.93
4	1071	562	$9.72 \cdot 10^{-3}$	$1.53 \cdot 10^{-5}$	$9.53 \cdot 10^{-3}$	1.02
5	1412	736	$7.70 \cdot 10^{-3}$	$1.59 \cdot 10^{-5}$	$7.34 \cdot 10^{-3}$	1.05
6	1861	962	$5.64 \cdot 10^{-3}$	$1.54 \cdot 10^{-5}$	$5.45 \cdot 10^{-3}$	1.04
7	2453	1262	$4.35 \cdot 10^{-3}$	$1.74 \cdot 10^{-5}$	$4.23 \cdot 10^{-3}$	1.03
8	3230	1660	$3.37 \cdot 10^{-3}$	$1.24 \cdot 10^{-5}$	$3.28 \cdot 10^{-3}$	1.03
9	4328	2214	$2.63 \cdot 10^{-3}$	$3.57 \cdot 10^{-6}$	$2.52 \cdot 10^{-3}$	1.04
10	5780	2946	$1.97 \cdot 10^{-3}$	$2.34 \cdot 10^{-6}$	$1.91 \cdot 10^{-3}$	1.03
11	7659	3890	$1.46 \cdot 10^{-3}$	$4.80 \cdot 10^{-6}$	$1.43 \cdot 10^{-3}$	1.02
12	10185	5168	$1.11 \cdot 10^{-3}$	$3.16 \cdot 10^{-6}$	$1.10 \cdot 10^{-3}$	1.01

TABLE 2: *Disparate meshes* $\mathcal{T}_P$ *and* $\mathcal{T}_M$

#	D_{P}	D_{M}	L_{P}	L_{M}	$L(\hat{e})$	θ
1	545	290	$2.81 \cdot 10^{-2}$	$1.27 \cdot 10^{-4}$	$3.15 \cdot 10^{-2}$	0.90
2	739	308	$2.35 \cdot 10^{-2}$	$9.37 \cdot 10^{-5}$	$1.98 \cdot 10^{-2}$	1.19
3	1001	336	$9.06 \cdot 10^{-3}$	$7.26 \cdot 10^{-5}$	$1.05 \cdot 10^{-2}$	0.87
4	1409	382	$7.36 \cdot 10^{-3}$	$1.95 \cdot 10^{-5}$	$7.21 \cdot 10^{-3}$	1.02
5	1933	438	$5.24 \cdot 10^{-3}$	$1.41 \cdot 10^{-5}$	$5.16 \cdot 10^{-3}$	1.02
6	2662	526	$4.07 \cdot 10^{-3}$	$1.81 \cdot 10^{-5}$	$3.94 \cdot 10^{-3}$	1.04
7	3615	650	$2.90 \cdot 10^{-3}$	$1.01 \cdot 10^{-5}$	$2.84 \cdot 10^{-3}$	1.03
8	4909	848	$2.32 \cdot 10^{-3}$	$5.47 \cdot 10^{-6}$	$2.25 \cdot 10^{-3}$	1.03
9	6558	1128	$1.71 \cdot 10^{-3}$	$9.98 \cdot 10^{-6}$	$1.69 \cdot 10^{-3}$	1.02
10	8638	1508	$1.32 \cdot 10^{-3}$	$7.14 \cdot 10^{-6}$	$1.31 \cdot 10^{-3}$	1.01
11	11483	1990	$1.02 \cdot 10^{-3}$	$4.19 \cdot 10^{-6}$	$1.01 \cdot 10^{-3}$	1.01

Iterations during adaptive procedure (unit square)

TABLE 3: *Common mesh* $\mathcal{T}$

#	D_{P}	D_{M}	L_{P}	L_{M}	$\lvert L_{\mathrm{P}}\rvert$	$\lvert L_{\mathrm{M}}\rvert$	$L(\hat{e})$	θ
1	833	450	$9.53 \cdot 10^{-3}$	$2.31 \cdot 10^{-3}$	$1.16 \cdot 10^{-2}$	$1.26 \cdot 10^{-2}$	$1.46 \cdot 10^{-2}$	0.81
2	1029	548	$7.25 \cdot 10^{-3}$	$2.32 \cdot 10^{-3}$	$8.66 \cdot 10^{-3}$	$1.11 \cdot 10^{-2}$	$1.17 \cdot 10^{-2}$	0.82
3	1304	688	$5.53 \cdot 10^{-3}$	$1.96 \cdot 10^{-3}$	$7.59 \cdot 10^{-3}$	$1.00 \cdot 10^{-2}$	$8.83 \cdot 10^{-3}$	0.85
4	1662	868	$4.29 \cdot 10^{-3}$	$1.53 \cdot 10^{-3}$	$6.18 \cdot 10^{-3}$	$8.46 \cdot 10^{-3}$	$6.81 \cdot 10^{-3}$	0.85
5	2147	1114	$3.30 \cdot 10^{-3}$	$1.13 \cdot 10^{-3}$	$5.07 \cdot 10^{-3}$	$7.71 \cdot 10^{-3}$	$5.05 \cdot 10^{-3}$	0.88
6	2798	1446	$2.57 \cdot 10^{-3}$	$1.01 \cdot 10^{-3}$	$4.06 \cdot 10^{-3}$	$6.92 \cdot 10^{-3}$	$4.11 \cdot 10^{-3}$	0.87
7	3635	1870	$2.06 \cdot 10^{-3}$	$7.67 \cdot 10^{-4}$	$3.62 \cdot 10^{-3}$	$6.20 \cdot 10^{-3}$	$3.17 \cdot 10^{-3}$	0.89
8	4774	2442	$1.58 \cdot 10^{-3}$	$6.14 \cdot 10^{-4}$	$3.17 \cdot 10^{-3}$	$5.44 \cdot 10^{-3}$	$2.50 \cdot 10^{-3}$	0.88
9	6268	3196	$1.25 \cdot 10^{-3}$	$4.42 \cdot 10^{-4}$	$2.62 \cdot 10^{-3}$	$4.60 \cdot 10^{-3}$	$1.87 \cdot 10^{-3}$	0.91
10	8164	4152	$9.68 \cdot 10^{-4}$	$3.32 \cdot 10^{-4}$	$2.25 \cdot 10^{-3}$	$4.08 \cdot 10^{-3}$	$1.42 \cdot 10^{-3}$	0.91
11	10600	5384	$7.76 \cdot 10^{-4}$	$2.61 \cdot 10^{-4}$	$1.84 \cdot 10^{-3}$	$3.61 \cdot 10^{-3}$	$1.11 \cdot 10^{-3}$	0.93

TABLE 4: *Disparate meshes* $\mathcal{T}_P$ *and* $\mathcal{T}_M$

#	D_{P}	D_{M}	L_{P}	L_{M}	$\lvert L_{\mathrm{P}}\rvert$	$\lvert L_{\mathrm{M}}\rvert$	$L(\hat{e})$	θ
1	833	450	$9.53 \cdot 10^{-3}$	$2.31 \cdot 10^{-3}$	$1.16 \cdot 10^{-2}$	$1.26 \cdot 10^{-2}$	$1.46 \cdot 10^{-2}$	0.81
2	1029	550	$7.31 \cdot 10^{-3}$	$2.16 \cdot 10^{-3}$	$8.65 \cdot 10^{-3}$	$1.06 \cdot 10^{-2}$	$1.17 \cdot 10^{-2}$	0.81
3	1296	702	$5.59 \cdot 10^{-3}$	$1.68 \cdot 10^{-3}$	$7.63 \cdot 10^{-3}$	$8.85 \cdot 10^{-3}$	$8.32 \cdot 10^{-3}$	0.87
4	1706	902	$4.00 \cdot 10^{-3}$	$1.36 \cdot 10^{-3}$	$5.59 \cdot 10^{-3}$	$7.82 \cdot 10^{-3}$	$6.38 \cdot 10^{-3}$	0.84
5	2133	1252	$3.07 \cdot 10^{-3}$	$1.06 \cdot 10^{-3}$	$4.46 \cdot 10^{-3}$	$7.13 \cdot 10^{-3}$	$4.71 \cdot 10^{-3}$	0.87
6	2711	1670	$2.52 \cdot 10^{-3}$	$8.57 \cdot 10^{-4}$	$3.78 \cdot 10^{-3}$	$6.16 \cdot 10^{-3}$	$3.93 \cdot 10^{-3}$	0.86
7	3339	2344	$2.07 \cdot 10^{-3}$	$6.11 \cdot 10^{-4}$	$3.31 \cdot 10^{-3}$	$5.05 \cdot 10^{-3}$	$3.13 \cdot 10^{-3}$	0.86
8	4469	3090	$1.60 \cdot 10^{-3}$	$4.71 \cdot 10^{-4}$	$2.88 \cdot 10^{-3}$	$4.41 \cdot 10^{-3}$	$2.35 \cdot 10^{-3}$	0.88
9	5961	4090	$1.20 \cdot 10^{-3}$	$3.47 \cdot 10^{-4}$	$2.52 \cdot 10^{-3}$	$3.84 \cdot 10^{-3}$	$1.70 \cdot 10^{-3}$	0.91
10	7787	5436	$9.45 \cdot 10^{-4}$	$2.73 \cdot 10^{-4}$	$1.96 \cdot 10^{-3}$	$3.41 \cdot 10^{-3}$	$1.34 \cdot 10^{-3}$	0.91
11	9845	7304	$7.49 \cdot 10^{-4}$	$2.07 \cdot 10^{-4}$	$1.67 \cdot 10^{-3}$	$2.95 \cdot 10^{-3}$	$1.07 \cdot 10^{-3}$	0.90

Iterations during adaptive procedure (L-shaped membrane)

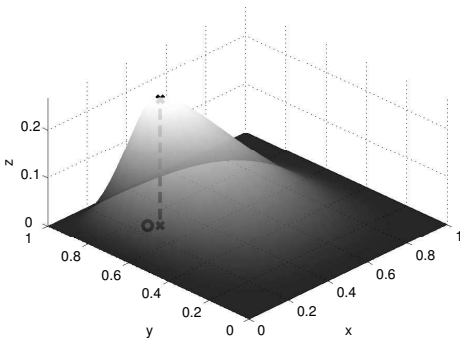

FIGURE 1: *Transversal plate deflection* u_h

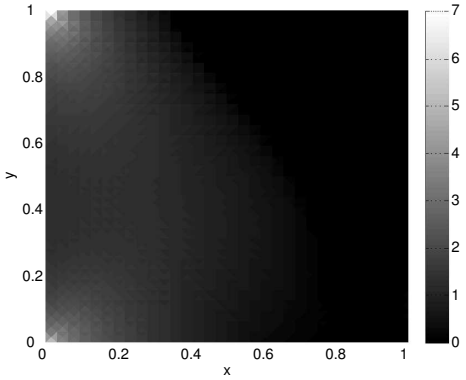

FIGURE 2: *Effective stress* $\boldsymbol{\sigma}_{\mathrm{e}}$

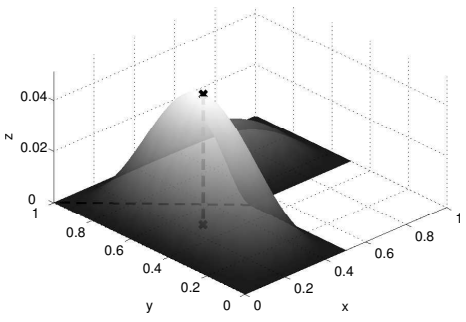

FIGURE 3: *Transversal plate deflection* u_h

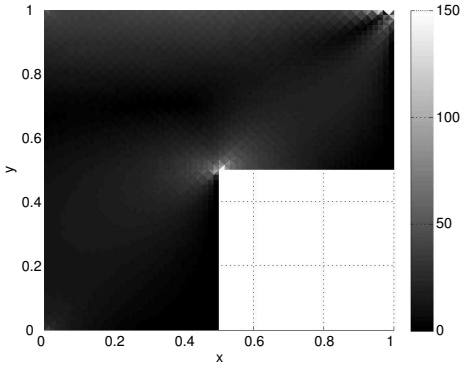

FIGURE 4: *Effective stress* $\boldsymbol{\sigma}_{\mathrm{e}}$

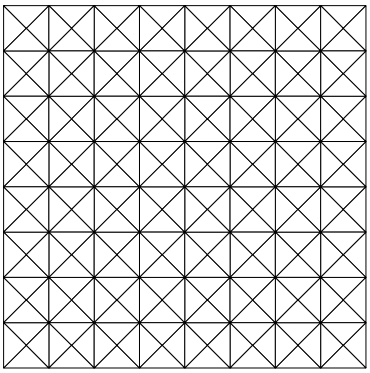

FIGURE 5: *Initial mesh $\mathcal{T}^0$ (always same)*

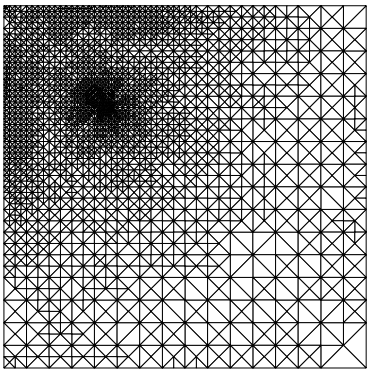

FIGURE 6: *Common mesh $\mathcal{T}^{12}$*

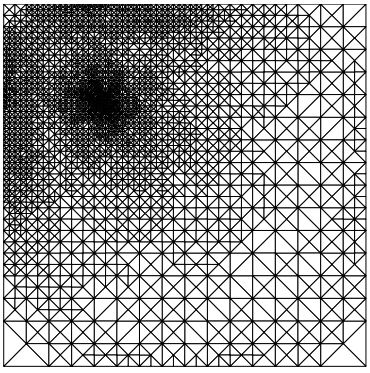

FIGURE 7: *Plate mesh $\mathcal{T}_P^{11}$*

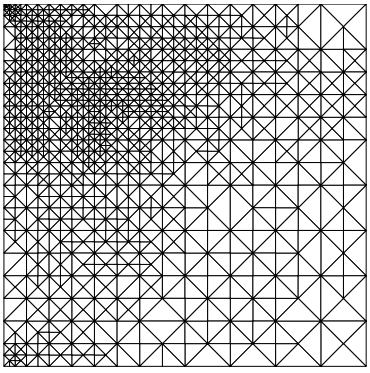

FIGURE 8: *Plane stress mesh $\mathcal{T}_M^{11}$*

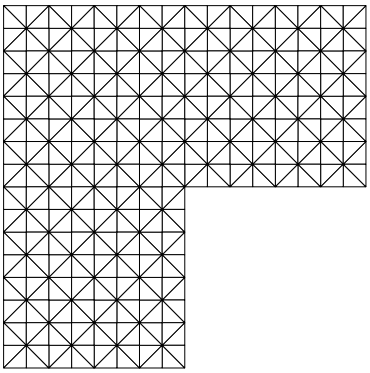

FIGURE 9: *Initial mesh* $\mathcal{T}^0$ *(always same)*

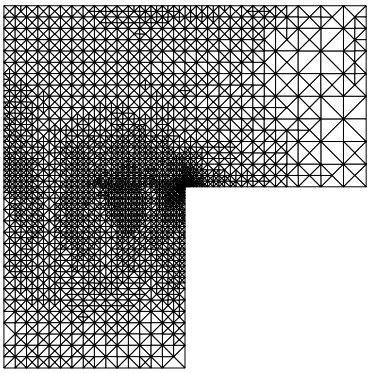

FIGURE 10: *Common mesh* $\mathcal{T}^{11}$

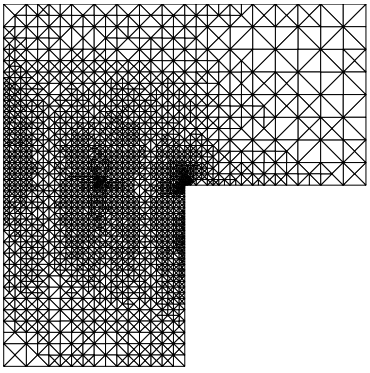

FIGURE 11: *Plate mesh* $\mathcal{T}_P^{11}$

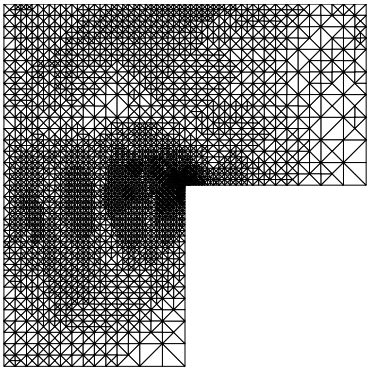

FIGURE 12: *Plane stress mesh* $\mathcal{T}_M^{11}$

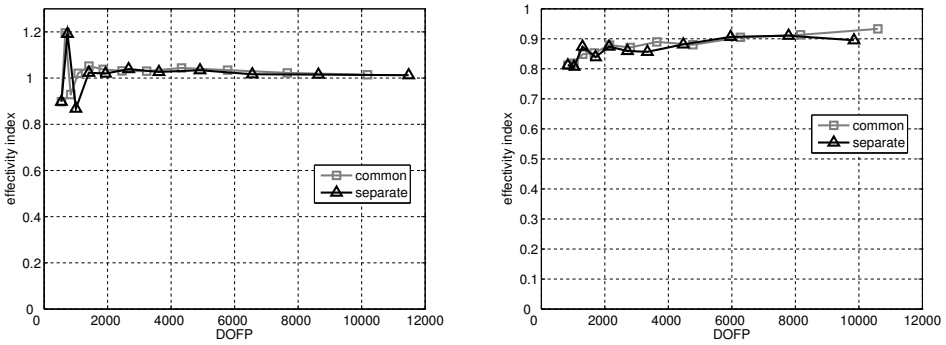

(a) *Unit square* (b) *L-shaped membrane*

FIGURE 13: *Effectivity indices (common mesh:* `com.`*; disparate meshes:* `disp.`*)*

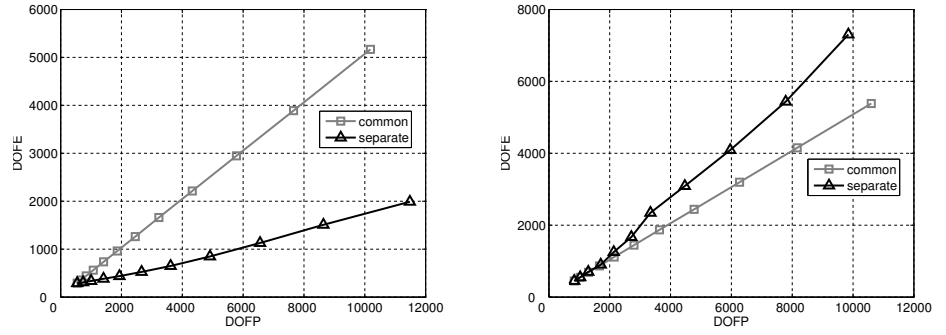

(a) *Unit square* (b) *L-shaped membrane*

FIGURE 14: *Distribution of degrees of freedom*

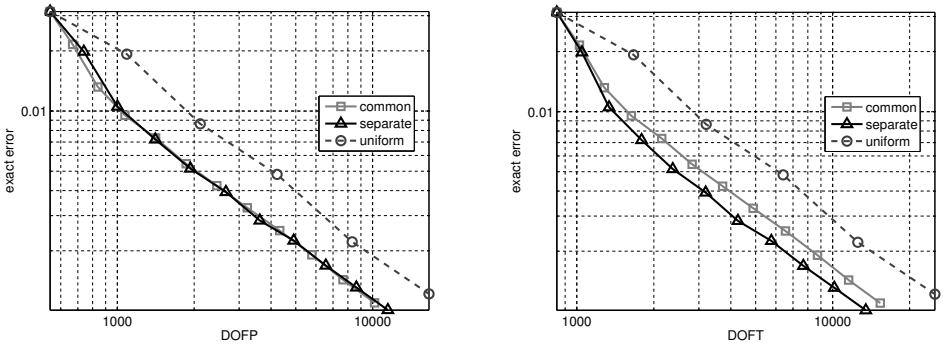

(a) *CM and DM are about equally accurate* (b) *DM uses a simpler model*

FIGURE 15: *Unit square (uniform mesh:* `uni.`*)*

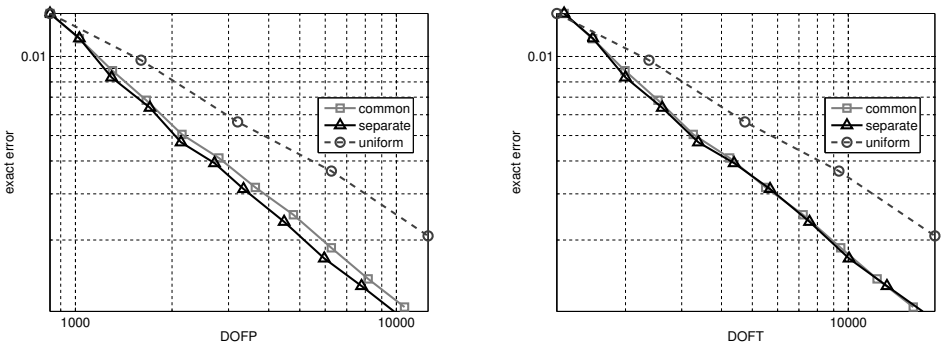

(a) *DM is the most accurate*

(b) *DM benefits from a more complex model*

FIGURE 16: *L-shaped membrane*